

## Article

# Study of Synthetic Titania Slags Demonstrating Characteristics Similar to High Titania Ilmenite Slag

Avishek Kumar Gupta<sup>1,\*</sup>, Matti Aula<sup>1</sup>, Harisankar Sreenivasan<sup>2</sup>, Pasi Mäkelä<sup>3</sup>, Marko Huttula<sup>4</sup> and Timo Fabritius<sup>1</sup>

<sup>1</sup> Process Metallurgy Research Unit, Faculty of Technology, University of Oulu, FI-90014 Oulu, Finland; matti.aula@oulu.fi (M.A.); timo.fabritius@oulu.fi (T.F.)

<sup>2</sup> Fibre and Particle Engineering Research Unit, University of Oulu, FI-90014 Oulu, Finland; harisankar.sreenivasan@oulu.fi

<sup>3</sup> Metso Outotec Research Centre, FI-28330 Pori, Finland; pasi.makela@mogroup.com

<sup>4</sup> Nano and Molecular Systems Research Unit, University of Oulu, FI-90014 Oulu, Finland; marko.huttula@oulu.fi

\* Correspondence: avishek.gupta@oulu.fi; Tel.: +358-46-9231-085

**Abstract:** The upgradation of the ilmenite ore, using a pyrometallurgy method, is performed using a carbothermic reduction of the ilmenite. A high titania slag is obtained which is used as a feedstock for the TiO<sub>2</sub> pigment production. The slag is cooled after tapping in big molds and can take ten days to cool. This cooling method has remained the same since the inception of ilmenite smelting and recently rapid cooling through granulation has been utilized. The work presented in this paper focuses on the microstructural study of the slags that were prepared using different techniques and cooled at different cooling rates. Various analytical techniques, such as X-ray powder diffraction (XRD), scanning electron microscopy (SEM), inductively coupled plasma-optical emission spectroscopy (ICP-OES), and X-ray photoelectron spectroscopy (XPS) were used to exhibit the similarity of these synthetic slags to the properties of high titania ilmenite slag. The slag consisted mostly of pseudo-brookite phase with a M<sub>3</sub>O<sub>5</sub> stoichiometry and smaller amounts of silicate and rutile phase. A glassy phase of silica was observed and most of the impurities were found to be present in the silicate phase. These silica phases were observed to be separate from the pseudo-brookite phase and along the phase boundaries. Micro-cracking of the slag surface, which is the characteristic of the M<sub>3</sub>O<sub>5</sub> phase formed in the ilmenite slag, were observed under the SEM analysis. The XPS analysis revealed that faster cooling does result in lower amount of oxidation but the difference in the TiO<sub>2</sub> and Ti<sub>2</sub>O<sub>3</sub> composition can have larger impact on oxidation than the cooling speed.

**Keywords:** titania slag; pseudo-brookite; slag cooling



**Citation:** Gupta, A.K.; Aula, M.; Sreenivasan, H.; Mäkelä, P.; Huttula, M.; Fabritius, T. Study of Synthetic Titania Slags Demonstrating Characteristics Similar to High Titania Ilmenite Slag. *Minerals* **2022**, *12*, 386. <https://doi.org/10.3390/min12030386>

Academic Editor: Jakub Kierczak

Received: 26 January 2022

Accepted: 17 March 2022

Published: 20 March 2022

**Publisher's Note:** MDPI stays neutral with regard to jurisdictional claims in published maps and institutional affiliations.



**Copyright:** © 2022 by the authors. Licensee MDPI, Basel, Switzerland. This article is an open access article distributed under the terms and conditions of the Creative Commons Attribution (CC BY) license (<https://creativecommons.org/licenses/by/4.0/>).

## 1. Introduction

Ilmenite is one of the major resources for titanium, the ninth most abundant element in the earth's crust [1]. As per U.S. Geological Survey (2021), ilmenite accounts for about 92% of the world's consumption of titanium minerals [2]. The major sources of TiO<sub>2</sub> are natural rutile, synthetic rutile, and high titanium slag [3]. Production of synthetic rutile includes the processes to remove iron from ilmenite giving a concentrate containing about 92% TiO<sub>2</sub> [4,5]. These are mainly solid-state reduction reactions, whereas high titanium slag is obtained by smelting ilmenite in an electric arc furnace at a relatively higher temperature of around 1650 °C to produce pig iron and high titanium slag containing 85–90% TiO<sub>2</sub> [6]. The high titania slag is used as a feed material for TiO<sub>2</sub> pigment production.

In this high-temperature electro-thermal smelting of ilmenite, the feed of ilmenite melts and the oxides of iron and titanium are reduced to produce a high titania slag and pig iron as the by-product. The high titania slag contains concentrates of FeO, Ti<sub>2</sub>O<sub>3</sub>, and TiO<sub>2</sub>. The smelting process of ilmenite is one unusual case where slag is the primary product

and metal is the by-product. The titanium slag is very aggressive and may damage the refractory lining of the furnace. To protect the refractory, a freeze lining of the solidified slag is used during the ilmenite process. The two basic reactions in ilmenite smelting are [7]:

Reduction of FeO from the slag:



Partial reduction of TiO<sub>2</sub> in the slag:



The metal bath is maintained at a lower temperature than the melting point of the slag and it is suggested that the partial solidification of the slag close to the metal bath happens with remelting of the slag [8,9]. As a result of the solidification equilibrium with the freeze lining in the furnace, the Fe is removed from the slag and it drives the slag to a characteristic composition of M<sub>3</sub>O<sub>5</sub> (pseudo-brookite) stoichiometry [10]. The solidified slag consists mostly of the M<sub>3</sub>O<sub>5</sub> (pseudo-brookite) solid-solution phase, contributing about 90% of the slag, and other phases such as anatase, rutile, iron titanium oxide and iron oxide [11]. M<sub>3</sub>O<sub>5</sub> is a molten mixture of Ti<sub>3</sub>O<sub>5</sub>, FeTi<sub>2</sub>O<sub>5</sub>, MnTi<sub>2</sub>O<sub>5</sub>, Al<sub>2</sub>TiO<sub>5</sub>, MgTi<sub>2</sub>O<sub>5</sub>, V<sub>2</sub>TiO<sub>5</sub> and Cr<sub>2</sub>TiO<sub>5</sub> in a solid solution [12]. This solid solution doesn't accommodate SiO<sub>2</sub>. SiO<sub>2</sub> forms a separate silicate phase together with the CaO, K<sub>2</sub>O and some of the Al<sub>2</sub>O<sub>3</sub> in the feed, which can be found in both crystalline and glassy phases. The silicates are located between the pseudo-brookite grains which is expected with the solidification of the slag. The silicates have a high SiO<sub>2</sub>/Al<sub>2</sub>O<sub>3</sub> ratio and show a lower melting behaviour compared to the pseudo-brookite phase which has a liquidus temperature of around 1600 °C. While cooling, pseudo-brookite starts forming just below 1600 °C and most of this phase is formed within 100 °C of cooling. Silicates, on the other hand, solidifies at much lower temperatures of around 1100–1300 °C [13].

Even though most of the phase present has the stoichiometric composition of M<sub>3</sub>O<sub>5</sub>, there is a small fraction of rutile (TiO<sub>2</sub>) in the slag. Rutile is formed in the solidified slag as a result of the oxidation that happens while tapping. If the slag is oxidized in the molten state, the slag deviates from the stoichiometric M<sub>3</sub>O<sub>5</sub> composition and as a result the rutile phase is formed as one of the solidification products. In addition to that, TiO<sub>2</sub> can exist in two non-equilibrium phases as anatase and brookite. Between the mono-oxide (TiO) and TiO<sub>2</sub> there are several phases with the stoichiometry Ti<sub>n</sub>O<sub>2n-1</sub>, where  $n > 1$ , which are called magneli phases.

In industry, the conventional way to cool the molten slag is to cast the liquid slag from the smelter into cup-shaped ingot molds, having typically a capacity of 20 to 25 tons. The slags can be air-cooled for around five days in the mold before they are crushed and milled into final products, or they can be cooled for two days in the mold with water cooling then tipped out of the molds and cooled further with water sprays. The cooling method, whether air or water cooling, does not significantly change the solidification rate of the industrial slag block [14]. The whole process can take almost 10 days to cool down and prepare the ilmenite slag for the next stage. To this date, the cooling method has remained unchanged in most industrial use though recently there has been trials of rapid cooling of the slags by granulation. Granulation can reduce the processing time of the slag and eliminate several crushing steps but there is a possibility that the granulated slag may react with water or oxygen during the cooling process [15]. It has been reported that the amount of Ti<sub>3</sub>O<sub>5</sub> decreases by around 5% in granulated slag when compared to the slag that has been cooled in the molds [16]. This is due to the oxidation of the slag during granulation and such oxidation can change the phases present in the slag [17]. As the Ti<sub>2</sub>O<sub>3</sub> is oxidized, it will result in the formation of tetravalent titanium-containing phase such as rutile thus increasing the amount of rutile that was already present in the slag composition. This

increase in rutile content (and decrease in pseudo-brookite) may affect the chlorination behavior of the slag, which is a process to further upgrade the slag to get  $\text{TiO}_2$  pigment.

Microcracks within the pseudo-brookite are a characteristic of the solidified titania slag. Microcracking is found on the surface of the slag and in the bulk too. Microcracking is found in the solidified slag because of the anisotropy of the thermal expansion coefficients [18,19]. Large differences in the thermal expansion coefficients were reported for temperatures around 400 °C. The cracks on the surface can occur due to the low-temperature oxidation but the cracks present throughout the bulk material can only be attributed to the thermal expansion coefficients and the thermal strain [20,21]. Low-temperature oxidation occurs around 400 °C which results in micro-cracking on the slag surface. To suppress this oxidation in industrial production, the slag is often cooled by water sprays to bring down the temperature below 400 °C.

In this study, slag samples originating from different slag preparation procedures are investigated to observe the difference in composition of the slags and the microstructural differences. These slags are produced using a pilot furnace and a laboratory induction furnace with different cooling procedures used for each type of slag. The slag samples were studied to analyze if their main titanium-containing phase follows  $\text{M}_3\text{O}_5$  stoichiometry characteristic to titania slag. Other characteristics such as the presence of a glassy phase of silica, rutile and micro-cracks within the pseudo-brookite phase were studied to demonstrate that different methods can be used to produce the high titania ilmenite slag.

## 2. Experimental Details

### 2.1. Sample Material

Four different kinds of ilmenite slag samples were used for this study which consisted of ladle cooled samples, granular samples, dip-rod samples and laboratory slag samples. Two samples of each kind were used, making it a total of eight samples. Sample 1 & 2 are the ladle cooled samples, 3 & 4 are the granular slag samples, 5 & 6 are the dip rod slag samples and 7 & 8 are the laboratory slag samples. The samples in each lot differ in composition from each other. The ladle cooled samples, granular samples and the dip-rod samples were provided by Metso Outotec and obtained from their pilot furnace whereas the laboratory slag was produced using a mixture of reagents in an induction furnace. Figure 1 shows the different kind of samples that were used for this study.

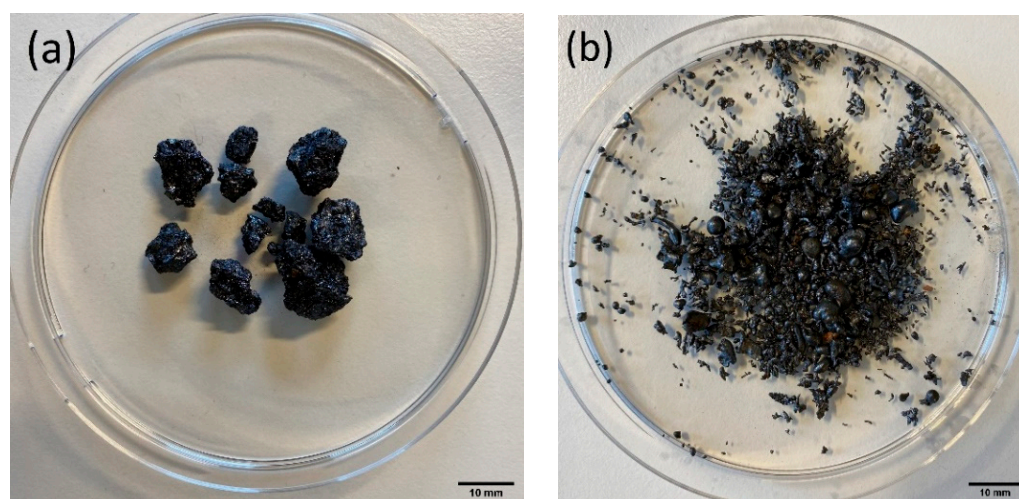
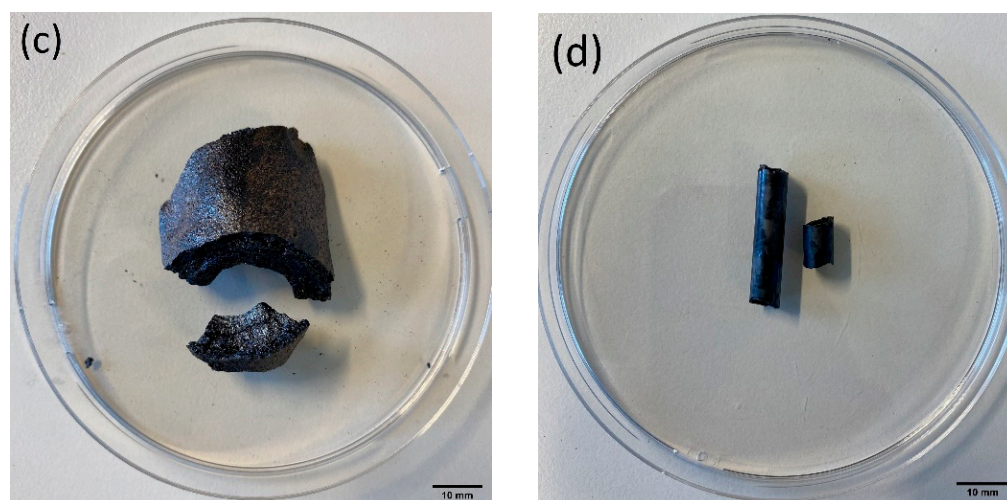


Figure 1. Cont.



**Figure 1.** Different kind of samples that were used in the study: (a) Ladle slag sample; (b) Granular slag sample; (c) Dip rod slag sample; (d) Laboratory slag sample.

Except the laboratory slag, the other slags were prepared by a carbothermic reduction of the ilmenite ore in a pilot furnace. The slags were collected and cooled in different ways thus the different kind of slags. The ladle-cooled samples were slowly cooled in the air atmosphere in the ladle after collecting them from the pilot furnace. The granular slag samples, on the other hand, were granulated by wet granulation and the samples were taken from the granulation pool. The dip rod samples were taken from inside the furnace during the ilmenite smelting and were allowed to cool in air atmosphere. For the laboratory slag preparation, the reagents were weighed and thoroughly mixed and the mixture was then charged in a 125 mL molybdenum crucible, which was placed in the induction furnace. Argon gas with a flow rate of 1 litre/min was purged above the insulating wool and inside the crucible to ensure an inert gas atmosphere that will prevent any oxidation of molybdenum crucible at a higher temperature. A quartz tube was used to take a sample of the molten slag from the crucible which was quenched in a cold-water bucket. The details of the laboratory slag preparation can be found in the work done by Gupta et al. [22]. Samples were selected for a wide range of  $\text{TiO}_2$ ,  $\text{MgO}$ , and  $\text{FeO}$  concentrations. Each sample was turned into a fine powder using ball milling.

## 2.2. Analytical Techniques

A Rigaku Smartlab 9 kW X-ray powder diffraction (XRD, Rigaku, Tokyo, Japan) was used for sample phase identification. The instrument is made of Bragg-Brentano parafocusing geometry (300 mm goniometer) and a Cu source lamp with 45 kV and 200 mA settings (9 kW rotating anode) with an acquisition speed of  $3^\circ$  per minute with  $0.02^\circ$  per step. The weight percentage of the phases present in the samples were analyzed using a PDXL2 software (Version 2.8, Rigaku, Japan) suite with integrated available PDF-4 2018 database. A Panalytical Axios Max model consisting of an X-ray generator Rh tube and a maximum power of 4 kW was used for the X-ray fluorescence (XRF) analysis of the powdered slag samples. The XRF provides the weight percentage of the identified elements. Fused bead samples were used for the measurement and the beads were produced using the Claisse Eaogn 2 fusion machine. The software, SuperQ 5.3, was used for the elemental analysis. The WROXI standard, which enables calibration for major elements in the analysis of oxide materials based on fused beads, was used as it produces consistently high-quality major and minor element analyses.

The elemental components of the slag were measured using a Thermo Scientific iCAP 7000 inductively coupled plasma analyzer (Thermo Fisher Scientific, Cambridge, UK) equipped with optical emission spectroscopy (ICP-OES). The slag was analyzed after the total dissolution of the sample to an acid mixture consisting of nitric acid, hydrochloric

acid and perchloric acid. The metallic iron was analyzed with ICP-OES after dissolution to bromine methanol whereas the trivalent titanium content was analyzed by a titration-based method from a precipitate of dissolution of the sample to bromine methanol. It is because the metallic iron disturbs this titration method. In addition, the  $\text{SiO}_2$  present in the samples were analyzed calorimetrically using a siliconmolybdene blue with Skalar Segmented Flow Analyzer (SFA San++, Skalar, Breda, Netherlands). The dissolution of the sample to NaOH melt and dilute hydrochloric acid was followed by the reduction with ascorbic acid. Skalar is an automated spectrophotometric analyzer used at UV/Vis region in this analysis method.

Scanning electron microscopy (SEM, ZEISS, Oberkochen, Germany) with backscattered electron imaging was used for the chemical characterization of the slag samples. Backscattered electron imaging was used to obtain the atomic number contrast in the microstructural image. X-ray photoelectron spectroscopy (XPS, Thermo Fisher Scientific, Cambridge, UK) analysis was conducted to provide information about the binding energy and the chemical state of the iron oxides. The XPS was carried on using a Thermo Fisher Scientific ESCALAB 250Xi XPS system. Monochromatized Al  $K\alpha$  was used to irradiate the sample and for the purpose of calibration, the binding energy adventitious carbon ( $C_{1s} = 284.8$  eV) was used. The samples were placed with a survey scan passing energy of 150 eV and an X-ray spot size of 900  $\mu\text{m}$ .

### 3. Results and Discussion

#### 3.1. Chemical Composition

The chemical composition of the titania slag samples measured using the ICP-OES, wet chemical analysis and coulometric analysis are listed in Table 1. The elemental composition obtained by ICP-OES was converted into weight percentages. XRF is also a measurement technique to get the weight percentage of the elements and is a simpler technique. XRF studies were conducted on the slag samples for comparison and the results are presented in Table 2. The titanium equivalent in the Table 1 represents the summation of  $\text{TiO}_2$  and  $\text{Ti}_2\text{O}_3$  in the slag. The XRF analysis for the titania oxides equivalent are similar to the values obtained by the ICP-OES analysis with a maximum percentage error of 4.5%. The mean absolute error for titanium oxide was 0.8 whereas for the iron and magnesium oxides it was 0.2 and 0.1 respectively. The error signifies the deviation of the XRF results from the results obtained from ICP-OES. The absolute error for the silicon and the aluminium oxides were 0.9 and 0.2 respectively, which is on the higher side considering that these impurities were present in a small quantity. In industrial application, ICP-OES is a standard measurement technique for elemental analysis for titania slag. The XRF gives good composition results for titanium oxides but not minor impurities, which can be a limitation for its application for titania slag analysis. The other impurities present in the slag such as vanadium oxide and chromium oxide were not taken into consideration as they are present in a very small quantity.

**Table 1.** Weight percentage of each component in the slag samples measured using ICP-OES. The trivalent titanium content was analyzed by a titration-based method.  $\text{SiO}_2$  was measured using Skalar Segmented Flow Analyzer (SFA San++).

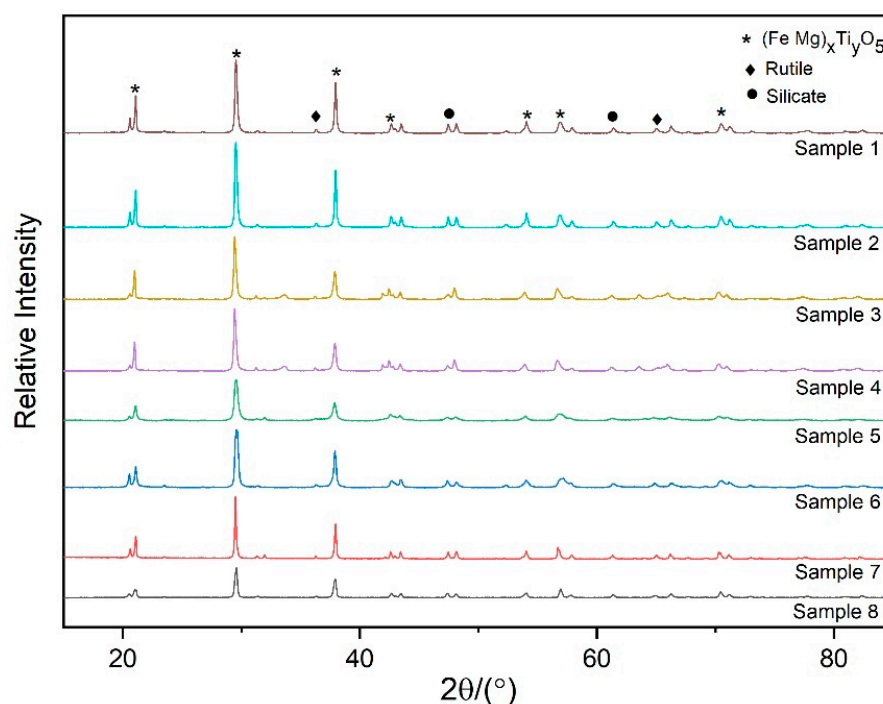
Sample	Weight Percentage of Each Component							Total
	$\text{TiO}_2$	$\text{Ti}_2\text{O}_3$	FeO	MgO	$\text{SiO}_2$	MnO	$\text{Al}_2\text{O}_3$	
1	63.7	13.7	8.0	8.6	1.4	1.7	2.9	100
2	60.8	20.7	11.9	1.9	1.1	1.6	2.1	100
3	66.0	17.0	11.6	1.1	1.2	1.3	1.8	100
4	52.6	34.7	7.1	1.1	1.2	1.2	2.1	100
5	56.4	23.6	4.1	7.2	2.6	1.5	4.6	100
6	57.1	22.8	4.3	7.1	2.7	1.5	4.5	100
7	59.4	15.8	14.0	5.4	2.2	0.3	2.9	100
8	60.7	22.5	7.4	4.9	1.9	0.6	2.0	100

**Table 2.** XRF analysis of different ilmenite slag samples.

Sample	Weight Percentage of Each Component						Total
	TiO <sub>2</sub> (Eq.)	FeO	MgO	SiO <sub>2</sub>	MnO	Al <sub>2</sub> O <sub>3</sub>	
1	76.9	9.4	7.2	2.1	1.5	2.9	100
2	81.9	10.6	1.9	2.0	1.5	2.1	100
3	86.9	7.2	1.2	1.8	1.3	1.6	100
4	87.0	7.1	1.2	1.8	1.3	1.6	100
5	76.5	6.1	8.1	3.4	1.5	4.4	100
6	76.5	6.0	8.1	3.5	1.5	4.4	100
7	74.0	15.3	4.4	3.6	0.4	2.3	100
8	81.5	8.5	4.5	3.2	0.6	1.7	100

### 3.2. Phase Analysis

The XRD pattern of the slag samples are illustrated in Figure 2. The XRD peaks of the pseudo-brookite phase match well with the standard given in the JCPDS database whereas additional peaks of rutile and silicate can be observed too. The most common phases that appeared in the XRD patterns are the pseudo-brookite, rutile, anatase and silicates. The M<sub>3</sub>O<sub>5</sub> (pseudo-brookite) phase in the slag is a solid solution of a mixture of Ti<sub>2</sub>FeO<sub>5</sub>, Mg<sub>0.5</sub>Ti<sub>2.5</sub>O<sub>5</sub>, and Mg<sub>2.5</sub>Ti<sub>0.5</sub>O<sub>5</sub>, according to the XRD analysis. For simplicity, all the solid solution having the M<sub>3</sub>O<sub>5</sub> composition is referred to as pseudo-brookite in this work. The pseudo-brookite phase was consistent in all the slag samples along with the silicate phase. The other minor phase that was observed in a significant fraction in most of the samples was rutile. The presence of rutile in the slag indicates that the slag mixture contained a higher amount of TiO<sub>2</sub> than the required for a M<sub>3</sub>O<sub>5</sub> stoichiometry composition.

**Figure 2.** X-ray powder diffraction (XRD) patterns of sample 7 and sample 8.

The XRD analysis using the Rietfeld refinement was done to identify the phase and its quantity. The analysis results of all the slag sample types are shown in Table 3. The pseudo-brookite phase with M<sub>3</sub>O<sub>5</sub> composition of divalent and trivalent ions was consistent in all samples and was the major phase in all samples. The silicate phase contained all the SiO<sub>2</sub> together with Al<sub>2</sub>O<sub>3</sub>, MnO and minor amount of MgO and TiO<sub>x</sub>. The empirical formulas of some of the common and identified silica phases include Mg<sub>0.84</sub>Ti<sub>0.33</sub>Al<sub>0.33</sub>Si<sub>0.5</sub>O<sub>3</sub>,

$\text{Mg}_{1.9}\text{Ti}_{0.07}\text{Si}_{0.98}\text{O}_4$ ,  $(\text{Mg}_{1.78}\text{Fe}_{0.22})(\text{SiO}_4)$  and  $(\text{Mg}_{0.83}\text{Al}_{0.16})(\text{Si}_{0.5}\text{Ti}_{0.33}\text{Al}_{0.16})\text{O}_3$ . The weight percentage of the pseudo-brookite phase above 80% in all samples which is in line with the  $\text{M}_3\text{O}_5$  composition in industrial high titania slags. It is observed from the XRD that the slags that are relatively slowly cooled (ladle cooled slag) have a lower number of silicates present and a higher rutile content than the other slags. The higher rutile content in the ladle-cooled samples can be a result of the oxidation during tapping as it was the slowest cooling method whereas the other samples were relatively faster cooled and hence the lesser rutile formation.

**Table 3.** Phases in weight (percentage) detected by XRD for each sample using the Rietfeld refinement.

Slag Sample	Phases (wt%)					Total
	Pseudo-Brookite	Silicate	Rutile	Anatase	Iron	
1	89.9	4.5	5.5			100
2	89.1	10.9				100
3	84.9	5.1	7.0		3.0	100
4	84.0	5.0		8.3	2.7	100
5	93.0	7.0				100
6	86.1	13.9				100
7	88.2	11.5	0.3			100
8	84.8	12.3	2.9			100

### 3.3. SEM Analysis

The microstructure of the samples was studied by SEM analysis using the backscattered electron imaging. The different phases observed using SEM were also analyzed using energy dispersive X-ray spectroscopy (EDS) to study the elemental composition on each phase. Figure 3 shows the microstructure of a laboratory slag sample 8 observed under SEM, the enlarged view is at a  $4000\times$  magnification of the  $1000\times$  magnified image. As observed in Figure 3 and the XRD result for sample 8, the slag consists of majorly three phases namely pseudo-brookite, silicate and rutile. The SEM-EDS analysis of the slag sample 8 is shown in Figure 3b and Table 4 which indicates the presence of three phases. Pseudo-brookite is a major phase whereas silicates and rutile form the minor phases. The silicate phase, consisting of a lighter average atomic number, is the darkest and easy to differentiate from the pseudo-brookite phase. Majority of the impurities are present in the silicate phase as observed in Table 4. Rutile, a solidification product, is observed in most of the samples. The presence of a substantial amount of rutile indicates that oxidation of the slag has taken place, during or after solidification [23].

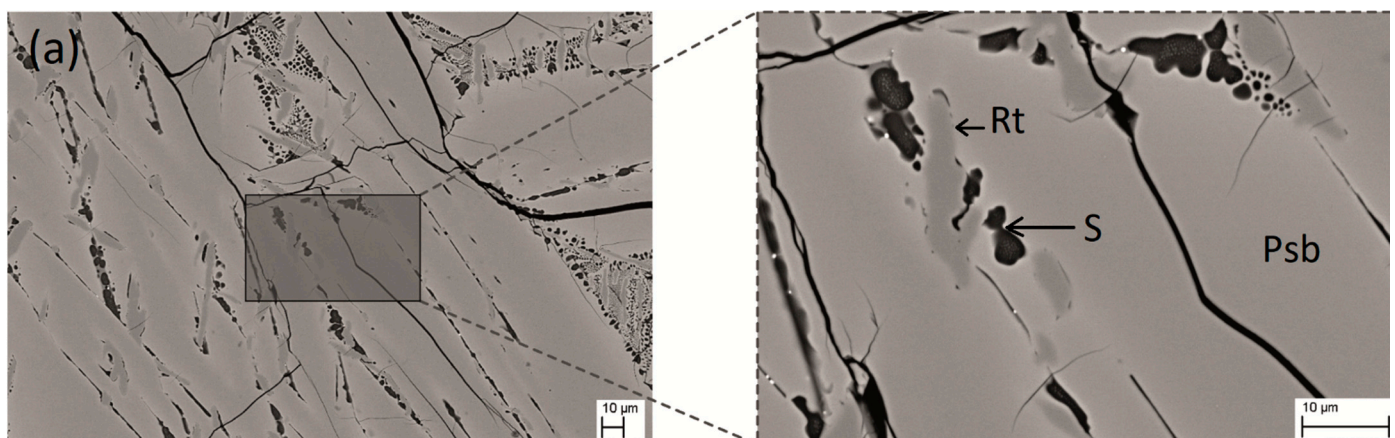


**Figure 3.** Cont.

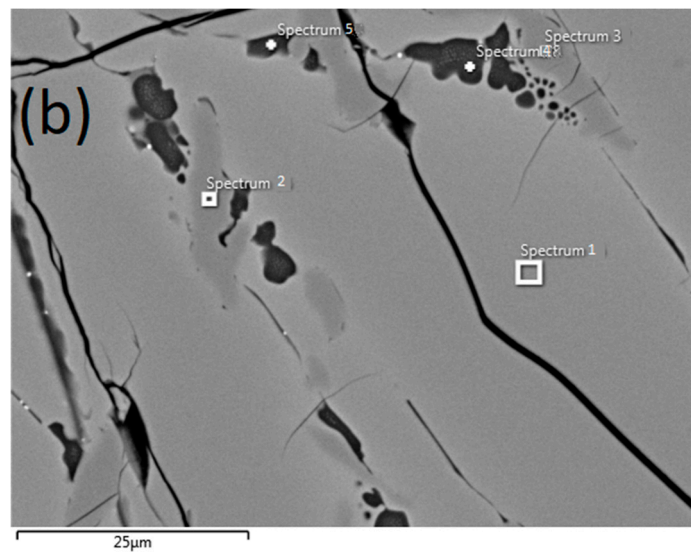


**Figure 3.** Microstructure of a laboratory slag Sample 8. (a) The figure shows the enlarged section of the slag sample at 4000 $\times$  magnification. The term 'Psb' indicates the  $M_3O_5$  (pseudo-brookite) phase, 'S' indicates silicates and 'Rt' indicates rutile phase. (b) SEM-EDS of the slag sample showing the areas of spectrum analysis.

**Table 4.** SEM-EDS analysis of the slag Sample 8 showing the elemental composition of various phases in the slag. The corresponding spectrum points can be observed in Figure 3b.

Element	Composition				
	Spectrum 1	Spectrum 2	Spectrum 3	Spectrum 4	Spectrum 5
O	37.70	39.89	40.13	48.25	47.07
Mg	3.78			0.79	0.76
Al	1.02			3.09	2.99
Si				24.78	23.66
Ti	52.95	60.11	59.87	15.87	19.18
Mn				1.43	1.27
Fe	4.55			5.80	5.09
Total	100	100	100	100	100

Visual inspection of the solid section indicates that most of the individual grains are needle-like in shape in most of the samples. The needle-like shaped grains can be observed in Figure 4 which shows the microstructure of the dip-rod slag sample. The elongated grains were less than an mm long and typically 50  $\mu\text{m}$  or less across.

Figure 5 shows the microstructure of all the slag samples at the same magnification. In most of the samples, small particles of metallic iron are found. The iron is mainly present in the rutile and the silica phase or at the boundary of pseudo-brookite phase with no visible presence within the pseudo-brookite phase. Upon close inspection, it is found that it contains traces of Ti-rich slag which is observed in the EDS-SEM analysis results showing a small presence of titanium in the iron particle. Almost all the  $\text{SiO}_2$  and the majority of  $\text{Al}_2\text{O}_3$  were present in the glass phase whereas the other impurities, such as  $\text{MnO}$  and  $\text{MgO}$ , were present in the pseudo-brookite and the silicate phases.

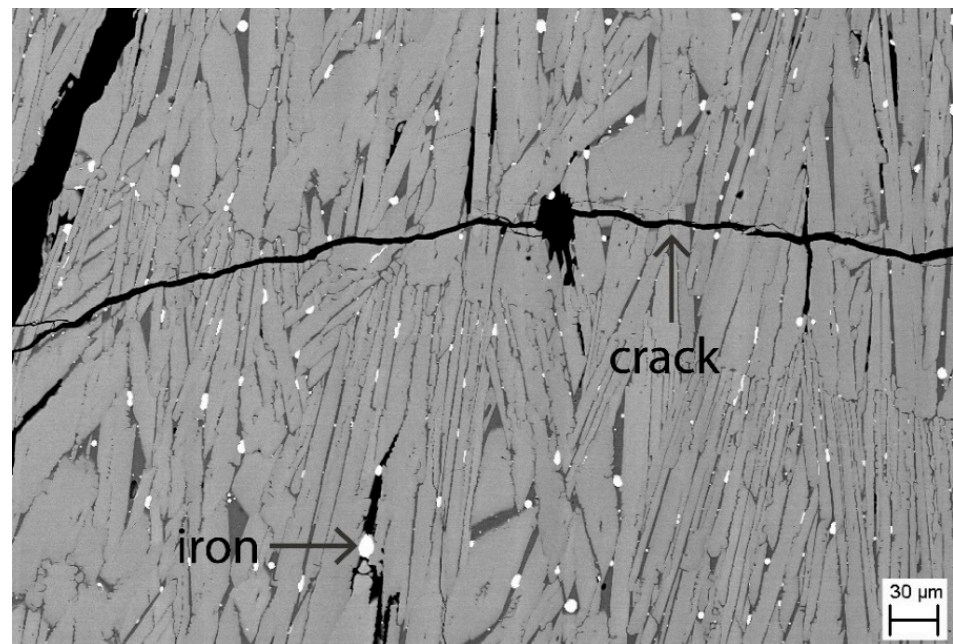


**Figure 4.** Microstructure of the dip-rod sample showing the elongated grains. The black lines are the cracks, and the white spots are metallic iron.

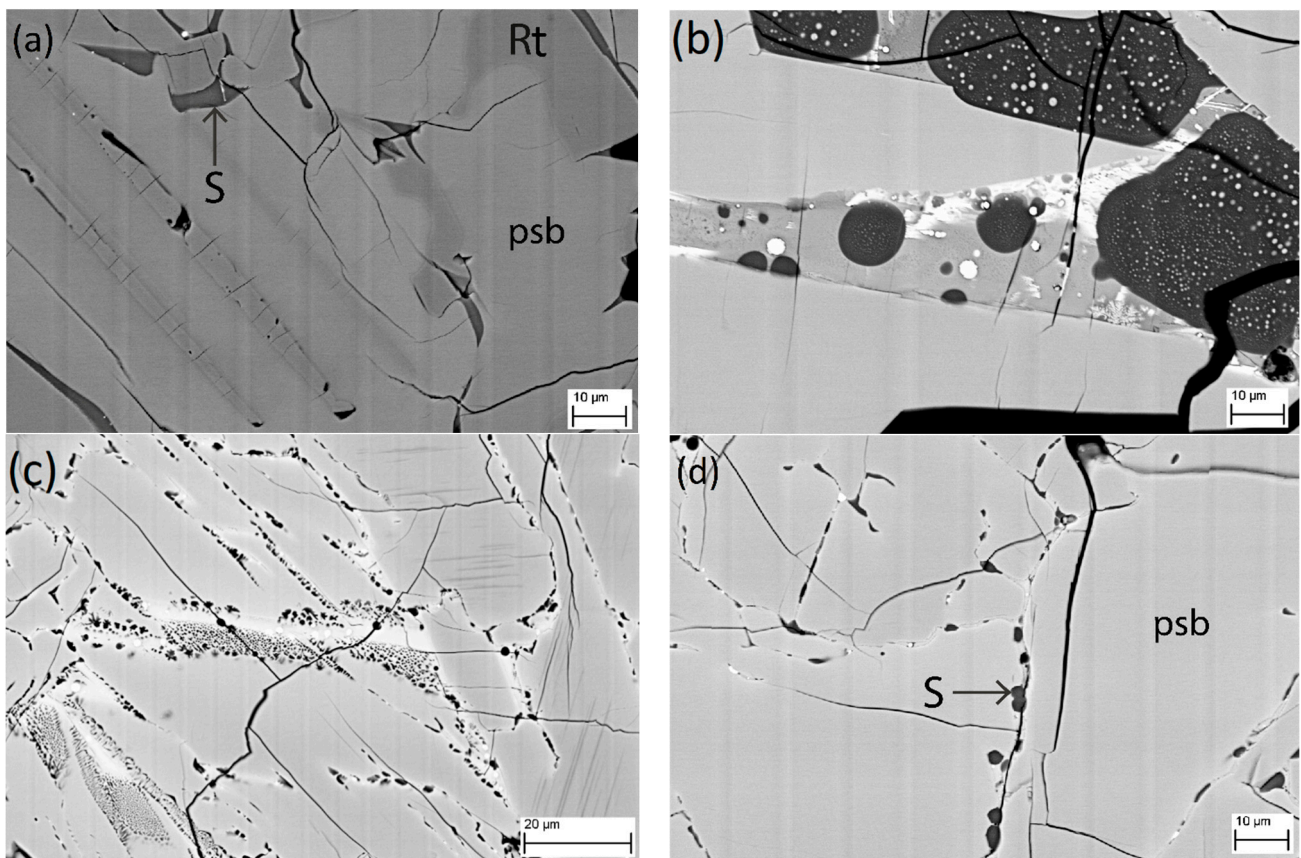


**Figure 5.** Cont.

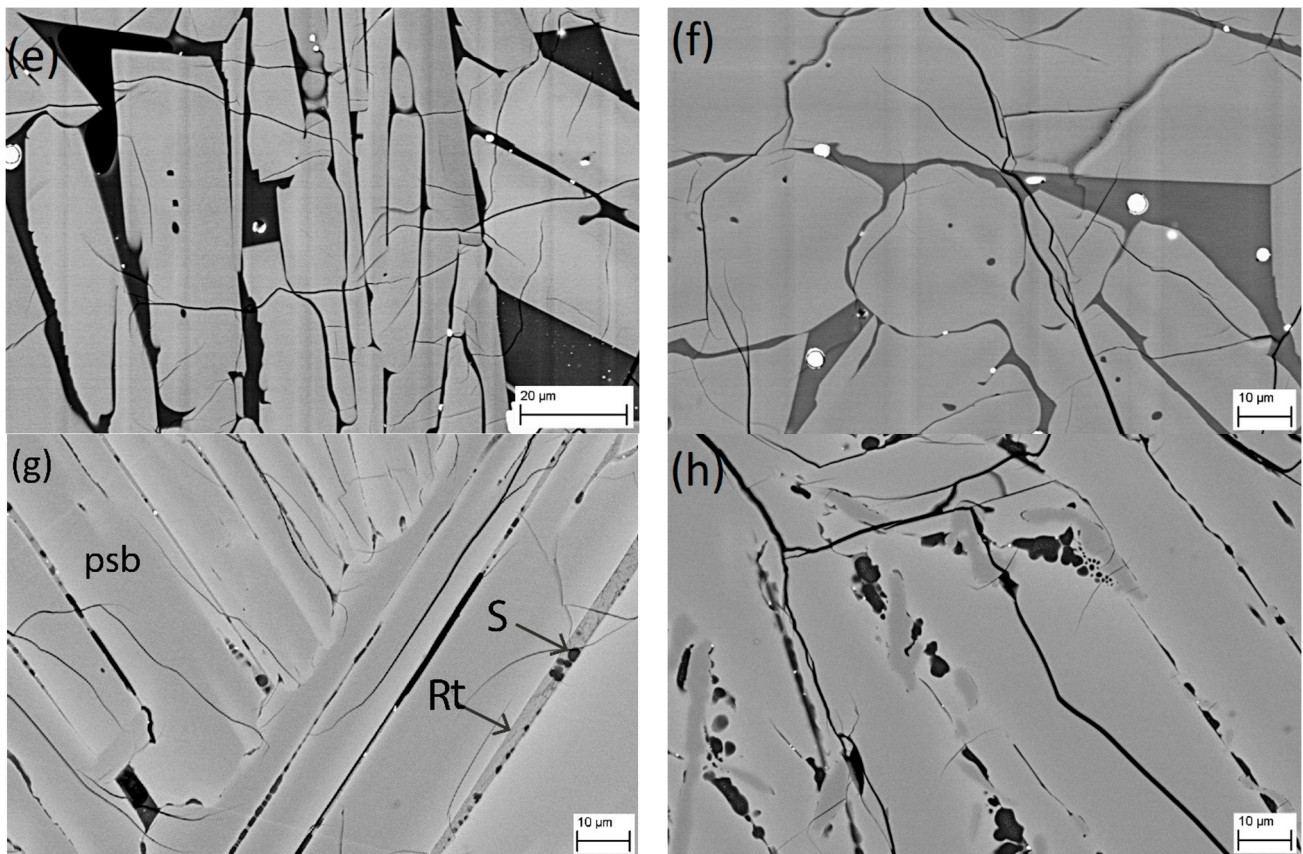


**Figure 5.** Microstructure of all the samples obtained with SEM at the same magnification of 2500 $\times$ . The darkest region indicates the silicate phase (S), the medium grey is rutile (Rt) and the lighter region is the pseudo-brookite (Psb). The black lines are the cracks present on the surface. (a) Sample 1 (b) Sample 2 (c) Sample 3 (d) Sample 4 (e) Sample 5 (f) Sample 6 (g) Sample 7 (h) Sample 8.

The SEM images show a wide range of microstructural arrangement for different samples which could be due to the differences in the method of sample preparation. For the dip-rod samples 5 and 6, the silicates are present in large quantities at fewer locations than compared to other samples where the silicates are distributed more evenly. The silicate phase observed in Figure 5e,f have accumulated between the pseudo-brookite phase resulting in a triangular shape. In the other samples the silicates are accumulated along the pseudo-brookite or rutile boundary in smaller quantities suggesting a large nucleating sites.

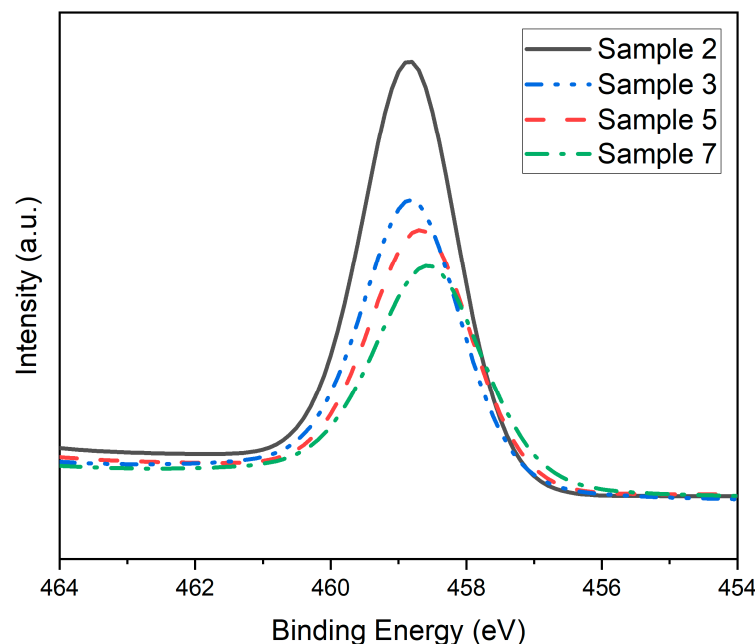
Major cracks are observed at lower magnification and upon further magnification, finer cracks are observed on the slag surface. Similar cracks are observed in all the slag samples, Figure 4, irrespective of the method of preparation. Microcracking in the pseudo-brookite is a common phenomenon and is attributed to the stress generated due to non-uniform thermal contraction of the pseudo-brookite phase while cooling.

### 3.4. XPS Analysis

The XPS analysis is a surface analytical technique in which the sample is irradiated with low-energy X-rays to provoke the photoelectric effect. The sampling depth is typically only a few nanometres and here it is used to find the binding energy of titanium in TiO<sub>2</sub>. Four different samples from each category of samples were analyzed using XPS. Table 5 gives the details of the binding energy and full width half maximum (FWHM) of the four different samples. One sample was selected from each category of sample preparation. The Ti 2p<sub>3/2</sub> binding energy for the four samples is represented in Figure 6.

**Table 5.** Binding energies and Full Width Half Maximum (FWHM) of different slag samples calculated using XPS.

Sample Type	Sample	Binding Energy (eV)	
		Ti 2p <sub>3/2</sub>	FWHM (eV)
Ladle cooled	2	458.82	1.70
Granular	3	458.79	1.72
Dip rod	5	458.66	1.82
Laboratory	7	458.54	1.88

**Figure 6.** Results of the XPS analysis showing the binding energy of the Ti 2p<sub>3/2</sub> for four samples from each category.

The identified Ti 2p<sub>3/2</sub> peaks at 458.82, 458.79, 458.66 and 458.54 eV for samples 2, 3, 5 and 7 respectively are similar to the locations at 458.6–459.5 eV found in published studies [24,25]. The binding energy is related to the electronic environment of the elements in study. The increase in binding energy in the XPS results corresponds to an increase in the oxidation state of the specimen. It is observed in Table 5 that the corresponding binding energy varies for all the different samples. The granular slag samples (samples 3 and 4) and the laboratory samples (samples 7 and 8) were produced using a faster quenching medium than the ladle (samples 1 and 2) and dip rod slags (samples 5 and 6). Oxidation happens during the cooling of the slag and different cooling techniques may alter the amount of oxidation in the specimen. The Ti<sup>4+</sup>/Ti<sup>3+</sup> ratio for the samples 2, 3, 5 and 7 are 10.1, 4.6, 2.8 and 2 respectively which signifies a big difference in the TiO<sub>2</sub> and Ti<sub>2</sub>O<sub>3</sub> composition in the titania slags. This difference may have played a bigger role in the difference in the amount oxidation of the specimen than the cooling speed. Additionally, the slag samples were prepared by ball milling and sometimes oxidation happens during the milling process due to the possible higher temperatures attained. Even though the slowest cooled and the fastest cooled slag satisfies the shift in binding energy, the complexity related to the amount of oxidation makes it difficult to relate the quenching speed with the shift in binding energy.

#### 4. Conclusions

Titania slags prepared using different methods, namely ladle cooled slag, granular slag, dip rod slag and laboratory slags were characterized using different techniques. The use of different techniques for slag preparation also utilized different cooling techniques.

The XRD analysis shows that the slowly cooled samples contain a higher rutile phase. The microstructure of the titania slag obtained using SEM agrees with the expected formation of silicates between the pseudo-brookite grains. In addition to the SEM, EDS results revealed that the pseudo-brookite phase contained some impurities including MgO and MnO but most of the impurities of the slag are present in the silicate phase. The pseudo-brookite grains are needle-like shaped with silicates present along the boundaries. Microcracking is observed in all the samples which is a characteristic feature of the high titania slag. The XPS was used to determine the binding energy of titanium. The shift in binding energy that corresponds to the oxidation of the slag was observed in a few samples. The  $Ti^{4+}/Ti^{3+}$  ratio obtained from XPS analysis reveals a large difference in composition of  $TiO_2$  and  $Ti_2O_3$ . This difference can have a major impact on the oxidation of the slags.

**Author Contributions:** Conceptualization, A.K.G. and M.A.; methodology, A.K.G. and M.A.; software, A.K.G. and H.S.; validation, M.A., P.M. and T.F.; formal analysis, A.K.G.; investigation, A.K.G. and M.A.; resources, P.M. and T.F.; data curation, A.K.G.; writing—original draft preparation, A.K.G.; writing—review and editing, M.A. and P.M.; visualization, A.K.G.; supervision, M.A., P.M. and T.F.; project administration, T.F. and M.H.; funding acquisition, T.F. and M.H. All authors have read and agreed to the published version of the manuscript.

**Funding:** This project has received funding from the European Union’s Horizon 2020 research and innovation programme under the Marie Skłodowska-Curie grant agreement No. 713606 under the I4Future doctoral programme—Imaging for the Future: Novel Imaging and Characterization Methods in Bio, Medical, and Environmental Research and Technology Innovations.

**Data Availability Statement:** All the data is contained within the article.

**Acknowledgments:** The authors acknowledge the support of the Academy of Finland projects (Academy of Finland, No. 311934 and No. 326291) and Metso Outotec (formerly Outotec) for their participation in the project.

**Conflicts of Interest:** The authors declare no conflict of interest.

## References

1. Mackey, T.S. Upgrading ilmenite into a high-grade synthetic rutile. *J. Miner. Met. Mater. Soc.* **1994**, *46*, 59–64. [[CrossRef](#)]
2. Gambogi, J. *Titanium Mineral Concentrates*; U.S. Geological Survey, Mineral Commodity Summaries, National Minerals Information Center: Lakewood, CA, USA, 2021. [[CrossRef](#)]
3. Sun, H.; Wang, J.; Dong, X.; Xue, Q. A literature review of titanium slag metallurgical processes. *Metal. Int.* **2012**, *17*, 49–56. [[CrossRef](#)]
4. Guo, Y.; Liu, S.; Jiang, T.; Qiu, G.; Chen, F. A process for producing synthetic rutile from Panzhihua titanium slag. *Hydrometallurgy* **2014**, *147–148*, 134–141. [[CrossRef](#)]
5. Liu, W.; Lü, L.; Yue, H.; Liang, B.; Li, C. Combined production of synthetic rutile in the sulfate  $TiO_2$  process. *J. Alloys Compd.* **2017**, *705*, 572–580. [[CrossRef](#)]
6. Ma, N.; Warner, N.A. Smelting reduction of ilmenite by carbon in molten pig iron. *Can. Met. Q.* **1999**, *38*, 165–173. [[CrossRef](#)]
7. Pistorius, P.C. Ilmenite smelting: The basics. *J. South. Afr. Inst. Min. Metall.* **2008**, *108*, 35–43.
8. Zietsman, J.H.; Pistorius, P.C. Process mechanisms in ilmenite smelting. *SIAMM J. South. Afr. Inst. Min. Metall.* **2004**, *104*, 653–660.
9. Pistorius, P.C.; De Villiers, J.P.R.; Gräser, P.; Venter, A. Partial slag solidification within ilmenite smelter. *Trans. Inst. Min. Met. C* **2011**, *120*, 211–217. [[CrossRef](#)]
10. Pistorius, P.C.; Coetzee, C. Physicochemical aspects of titanium slag production and solidification. *Met. Mater. Trans. B* **2003**, *34*, 581–588. [[CrossRef](#)]
11. Samal, S.; Mohapatra, B.; Mukherjee, P.; Chatterjee, S. Integrated XRD, EPMA and XRF study of ilmenite and titania slag used in pigment production. *J. Alloys Compd.* **2009**, *474*, 484–489. [[CrossRef](#)]
12. Guéguin, M.; Cardarelli, F. Chemistry and Mineralogy of Titania-Rich Slags. Part 1—Hemo-Ilmenite, Sulphate, and Upgraded Titania Slags. *Miner. Process. Extr. Met. Rev.* **2007**, *28*, 1–58. [[CrossRef](#)]
13. Fan, H.; Chen, D.; Liu, T.; Duan, H.; Huang, Y.; Long, M.; He, W. Crystallization Behaviors of Anosovite and Silicate Crystals in High CaO and MgO Titanium Slag. *Metals* **2018**, *8*, 754. [[CrossRef](#)]
14. Kotzé, H.; Pistorius, P.C. A heat transfer model for high titania slag blocks. *J. South. Afr. Inst. Min. Metall.* **2010**, *110*, 57–66.
15. Bessinger, D.; Beukes, P.; Glenewinkel, R. Granulation of titania slag. In *The 6th International Heavy Minerals Conference ‘Back to Basics’*; The Southern African Institute of Mining and Metallurgy: Johannesburg, South Africa, 2007; pp. 159–162.
16. Song, B.; Han, K.; Lv, X. Effect of Cooling Approaches on Chemical Compositions, Phases, and Acidolysis of Panzhihua Titania Slag. *Int. J. Mater. Metall. Eng.* **2017**, *11*, 736–741.

17. Bungu, P.; Pistorius, P. Mineralogy and Initial Chlorination of Water Granulated High Titania Slag. *Can. Met. Q.* **2009**, *48*, 45–52. [[CrossRef](#)]
18. De Villiers, J.P.R.; Göske, J.; Tuling, A. Disintegration in high grade titania slags: Low temperature oxidation reactions and associated fracture mechanics of pseudobrookite. *Trans. Inst. Min. Metall. Sect. C* **2005**, *114*, 73–79. [[CrossRef](#)]
19. Siebeneck, H.J.; Hasselman, D.P.H.; Cleveland, J.J.; Bradt, R.C. Effects of Grain Size and Microcracking on the Thermal Diffusivity of  $MgTi_2O_5$ . *J. Am. Ceram. Soc.* **1977**, *60*, 336–338. [[CrossRef](#)]
20. Pistorius, P.C.; Kotze, H. The Link Between Solidification of High-Titania Slag and Subsequent Comminution. In Proceedings of the VIII International Conference of Molten Slags, Fluxes & Salts, Santiago, Chile, 18–21 January 2009; pp. 51–60.
21. Siebeneck, H.J.; Hasselman, D.P.H.; Cleveland, J.J.; Bradt, R.C. Effect of Microcracking on the Thermal Diffusivity of  $Fe_2TiO_5$ . *J. Am. Ceram. Soc.* **1976**, *59*, 241–244. [[CrossRef](#)]
22. Gupta, A.K.; Aula, M.; Pihlasalo, J.; Mäkelä, P.; Huttula, M.; Fabritius, T. Preparation of Synthetic Titania Slag Relevant to the Industrial Smelting Process Using an Induction Furnace. *Appl. Sci.* **2021**, *11*, 1153. [[CrossRef](#)]
23. Pistorius, P.C.; Kotzé, H. Role of silicate phases during comminution of titania slag. *Miner. Eng.* **2009**, *22*, 182–189. [[CrossRef](#)]
24. Stefanov, P.; Shipochka, M.; Stefchev, P.; Raicheva, Z.; Lazarova, V.; Spassov, L. XPS characterization of  $TiO_2$  layers deposited on quartz plates. *J. Phys. Conf. Ser.* **2008**, *100*, 012039. [[CrossRef](#)]
25. Wang, Y.; Sun, H.; Tan, S.; Feng, H.; Cheng, Z.; Zhao, J.; Zhao, A.; Wang, B.; Luo, Y.; Yang, J.; et al. Role of point defects on the reactivity of reconstructed anatase titanium dioxide (001) surface. *Nat. Commun.* **2013**, *4*, 2214. [[CrossRef](#)] [[PubMed](#)]